1   **Revision 1**

2

3   **Jasonsmithite, a new phosphate mineral with a complex microporous**

4   **framework, from the Foote mine, North Carolina, U.S.A.**

5

6   ANTHONY R. KAMPF[1§], AARON J. CELESTIAN[1], AND BARBARA P. NASH[2]

7

8   [1]Mineral Sciences Department, Natural History Museum of Los Angeles County, 900 Exposition
9   Boulevard, Los Angeles, CA 90007, U.S.A.

10   [2]Department of Geology and Geophysics, University of Utah, Salt Lake City, Utah 84112, U.S.A.

11

12   ABSTRACT

13   Jasonsmithite (IMA2019–121), $Mn^{2+}_4ZnAl(PO_4)_4(OH)(H_2O)_7 \cdot 3.5H_2O$, is a pegmatite-

14   phosphate mineral from the Foote Lithium Company mine, Kings Mountain district, Cleveland

15   County, North Carolina, USA. It is is interpreted as having formed by late–stage, low–

16   temperature hydrothermal alteration. Crystals are colorless to light brown, slightly flattened

17   prisms to about 1 mm in length with wedge–shaped terminations. The mineral is transparent with

18   vitreous luster, white streak, Mohs hardness 2, brittle tenacity, irregular fracture, and perfect

19   {001} cleavage. The density is 2.63(2) g/cm^3. Jasonsmithite is biaxial (–), with $\alpha = 1.561(2)$, $\beta =$

20   1.580(2), $\gamma = 1.581(2)$, measured in white light. The 2V is 25(5)° and dispersion is $r < v$

§ *Email address:* akampf@nhm.org

21   moderate. The optical orientation is $Y = \mathbf{b}$, $X \wedge \mathbf{c} = 18°$ in obtuse β. The Raman spectrum is

22   dominated by vibrational modes of PO_4 and ZnO_4 tetrahedra, AlO_6 and MnO_6 octahedra, and OH

23   groups. Electron–microprobe analyses gave the empirical formula

24    $(Mn_{3.09}Fe_{0.87})_{\Sigma 3.96}Zn_{1.05}Al_{0.98}(PO_4)_4(OH)(H_2O)_7 \cdot 3.5H_2O$. The mineral is monoclinic, $P2_1/c$, $a =$

25   8.5822(3), $b = 13.1770(6)$, $c = 20.3040(14)$ Å, $\beta = 98.485(7)°$, $V = 2271.0(2)$ Å^3, and $Z = 4$.

26   The structure ($R_1 = 0.0443$ for 3685 $I > 2\sigma I$ reflections) contains zig–zag chains of edge–sharing

27   MnO_6 octahedra that corner link to adjacent chains and to PO_4 tetrahedra to form sheets, which

28   are decorated by ZnO_4 tetrahedra. The sheets are linked to one another *via* dimers of AlO_6

29   octahedra, forming a framework with large channels containing H_2O groups. With H_2O groups

30   removed, the framework has a void space of 70.2% per unit cell, and a framework density of 14.5

31   polyhedral atoms/1000 Å^3, which would place jasonsmithite among the most porous minerals.

32

33   Keywords: jasonsmithite; new mineral; phosphate; microporous framework structure;

34   Raman spectroscopy; Foote mine, Kings Mountain, North Carolina, U.S.A.

35

36   INTRODUCTION

37   The Foote Lithium Company mine in the Kings Mountain district, Cleveland County,

38   North Carolina (USA) exploits spodumene–bearing pegmatites that have yielded a wide variety

39   of rare silicate and phosphate minerals, among them 14 new mineral species. Herein, we describe

40   jasonsmithite, the 15th new mineral from the Foote mine.

41   The mineral is named 'jasonsmithite' in honor of American mineral collector Jason B.

42   Smith (b. 1977) of Charlotte, North Carolina, USA. Jason has long specialized in the minerals of

43   the Foote Lithium Company mine, where he has collected extensively. He is responsible for the

44   discovery of the new Foote–mine mineral species fanfaniite, ferraioloite, footemineite, and

45   kayrobertsonite, as well as for jasonsmithite. Jason Smith has given permission for this mineral to

46   be named in his honor.

47   The new mineral and name have been approved by the Commission on New Minerals,

48   Nomenclature and Classification of the International Mineralogical Association (IMA2019–121).

49   The holotype and two cotype specimens are deposited in the collections of the Mineral Sciences

50   Department, Natural History Museum of Los Angeles County, 900 Exposition Boulevard, Los

51   Angeles, California 90007, USA, catalogue numbers 74374 (holotype), 74375 (cotype), and

52   74376 (cotype).

53

54   <center>OCCURRENCE</center>

55   Jasonsmithite was found by Jason B. Smith on the East dump of the Foote Lithium

56   Company mine, Kings Mountain district, Cleveland County, North Carolina, USA (35°12'40"N,

57   81°21'20"W). A brief summary of the history and geology of the Foote mine was provided by

58   Rakovan et al. (2016). Jasonsmithite was found in solution fractures and small vugs of partially

59   oxidized pegmatite. The pegmatite matrix consists of albite, columbite–(Fe), ferrisicklerite,

60   fluorapatite, muscovite, quartz, sphalerite, and spodumene. The secondary association found in

61   vugs with jasonsmithite includes eosphorite, hureaulite, jahnsite–(MnMnMn), kastningite,

62   mangangordonite, metaswitzerite, nizamoffite, stewartite, variscite, and whiteite–(CaMnMn).

63   Jasonsmithite is interpreted as having formed by late–stage, low–temperature hydrothermal

64   alteration. The order of formation of secondary phases at the Foote mine typically follows a trend

65   defined by lowering temperature and concomitant increasing degree of hydration. For the

66   jasonsmithite association, the order from early to late is interpreted as (1) eosphorite, (2)

67   hureaulite, (3) nizamoffite, (4) metaswitzerite + jasonsmithite + mangangordonite + kastningite +

68   whiteite–(CaMnMn), (5) jahnsite–(MnMnMn) + stewartite + varsicite.

69

70   PHYSICAL AND OPTICAL PROPERTIES

71   Jasonsmithite crystals are slightly flattened prisms to about 1 mm in length with wedge–

72   shaped terminations. Elongation is parallel to [100] and flattening is on {001}. The crystal forms

73   are {010}, {001}, {011}, and {11–1} (Fig. 1). Crystals commonly occur in subparallel

74   intergrowths (Fig. 2). No twinning was observed. The color of prisms commonly varies from

75   colorless to light brown with indistinct color boundaries (Fig. 2). The cause of the color has not

76   been determined, although the appearance is what might be expected from indistinct

77   submicroscopic inclusions. No compositional variation that can be correlated with the color

78   variation was observed in the electron–probe microanalyses.

79   The streak is white, the luster is vitreous, and crystals are transparent. The mineral does

80   not fluoresce under long– or short–wave ultraviolet light. The Mohs hardness is about 2 based on

81   scratch tests. The tenacity is brittle, cleavage is perfect on {001}, and the fracture is irregular.

82   The density measured by flotation in methylene iodide – toluene is 2.63(2) g/cm^3. The calculated

83   density is 2.630 g/cm^3 for the empirical formula and 2.627 g/cm^3 for the ideal formula. At room

84   temperature, the mineral is easily soluble in dilute HCl.

85   Optically, the mineral is biaxial (–), with $\alpha = 1.561(2)$, $\beta = 1.580(2)$, $\gamma = 1.581(2)$,

86   measured in white light. The $2V$ was estimated as 25(5)° from conoscopic observation. The

87   calculated $2V$ is 25.6° Dispersion is $r < v$ moderate. The optical orientation is $Y =$ **b**, $X \wedge$ **c** $= 18°$

88   in the obtuse angle β. No pleochroism was observed.

89

90   RAMAN SPECTROSCOPY

91   Raman spectroscopy was done on a Horiba XploRa+ micro–Raman spectrometer using an

92   incident wavelength of 532 nm, laser slit of 50 μm, 2400 gr/mm diffraction grating, and a 100x

93   (0.9 NA) objective. The spectrum was recorded from 4000 to 60 cm^{-1}. It was featureless between

94   2500 and 1200 cm^{-1}. The spectrum from 4000 to 2500 cm^{-1} is shown as an insert in the spectrum

95   from 1200 to 60 cm^{-1} in Figure 3. A list of the band positions, HWHMs (half-width at half

96   maximum intensity), and integrated intensities is on deposit as Supplemental[1] Table S1.

97   The Raman spectrum of jasonsmithite is dominated by vibrational modes of the PO_4 and

98   ZnO_4 tetrahedra, the AlO_6 and MnO_6 octahedra, and the OH groups. The OH stretching

99   associated with H_2O and OH groups is dominant above 2200 cm^{-1} (see Figure 3 insert). The lack

100   of any apparent band around 1630 cm^{-1} corresponding to H_2O bending could be related to the

101   existence of many different H_2O sites (both on the framework and in the channel). These are

102   likely to result in many overlapping, broad low-intensity peaks, which we do not have the

103   resolution to observe, especially considering the high-background fluorescence in that region.

104   The stretching modes for the PO_4 and ZnO_4 overlap in the region at approximately 1050

105   to 900 cm^{-1}. Bending modes for PO_4 and ZnO_4, as well as the stretching modes for the AlO_6 and

106   MnO_6 groups are approximately located in the $700 – 400$ cm^{-1} region. Below 400 cm^{-1} is

107   dominated by octahedral bending vibrations and lattice vibrations. Because of the complexity of

108   the crystal structure, including the number of different polyhedra components within the structure

109   and the varying local geometry of those components, it is not possible at this time to identify the

110   precise vibrational mode for each peak in the Raman spectrum.

111

112   CHEMICAL COMPOSITION

113   Analyses (14 points on 2 crystals) were performed at the University of Utah on a Cameca

114   SX–50 electron microprobe with four wavelength dispersive spectrometers and using Probe for

115   EPMA software. Analytical conditions were 15 kV accelerating voltage, 10 nA beam current, and

116   a beam diameter of 10 μm. Raw X–ray intensities were corrected for matrix effects with a $\phi\rho(z)$

117   algorithm (Pouchou and Pichoir 1991); total oxygen, including H_2O, was used in matrix

118   corections. No other elements were detected by EDS or by WDS wave scans. There was only

119   minor damage from the electron beam. Because insufficient material is available for a direct

120   determination of H_2O, it has been calculated based upon the structure determination (P = 4 and O

121   = 27.5 apfu). The analytical results are provided in Table 1.

122   The empirical formula (based on 4 P and 27.5 O apfu) is

123    $(Mn_{3.09}Fe_{0.87})_{\Sigma3.96}Zn_{1.05}Al_{0.98}(PO_4)_4(OH)(H_2O)_7 \cdot 3.5H_2O$ (+0.05 H for charge balance). The

124   simplified formula is $(Mn^{2+},Fe^{2+})_4ZnAl(PO_4)_4(OH)(H_2O)_7 \cdot 3.5H_2O$. The ideal formula is

125    $Mn^{2+}_4ZnAl(PO_4)_4(OH)(H_2O)_7 \cdot 3.5H_2O$, which requires MnO 31.59, ZnO 9.06, Al_2O_3 5.68, P_2O_5

126   31.61, H_2O 22.06, total 100 wt%.

127   The Gladstone–Dale compatibility index $1 - (K_P/K_C)$ for the empirical formula is -0.010

128   indicating superior compatibility among the average index of refraction, calculated density, and

129   chemical composition (Mandarino 2007).

130

131   X–RAY CRYSTALLOGRAPHY AND STRUCTURE DETERMINATION

132   Powder X–ray studies were done using a Rigaku R–Axis Rapid II curved imaging plate

133   microdiffractometer, with monochromatized Mo$K\alpha$ radiation ($\lambda = 0.71075$ Å). A Gandolfi–like

134   motion on the ϕ and ω axes was used to randomize the samples. Observed d values and

135   intensities were derived by profile fitting using JADE 2010 software (Materials Data, Inc.

136   Livermore, CA). Data are given in Supplemental[2] Table S1. The observed powder diffraction

137   pattern compares very well with the pattern calculated from the crystal structure (Fig. 4). Unit

138   cell parameters refined from the powder data using JADE 2010 with whole pattern fitting are $a =$

139   8.574(5), $b = 13.168(5)$, $c = 20.387(5)$ Å, $\beta = 98.577(13)°$, and $V = 2276.0(17)$ Å^3.

140   Single–crystal data were collected using the same diffractometer and radiation noted

141   above. The Rigaku CrystalClear software package was used for processing the structure data,

142   including the application of an empirical absorption correction using the multi–scan method with

143   ABSCOR (Higashi 2001). The structure was solved by the charge–flipping method using

144   SHELXT (Sheldrick 2015a). Refinement proceeded by full–matrix least–squares on F^2 using

145   SHELXL–2016 (Sheldrick 2015b). A difference Fourier synthesis located most H atom positions,

146   which were then refined with soft restraints of 0.82(3) Å on the O–H distances and 1.30(3) Å on

147   the H–H distances and with the U_{eq} of each H set to 1.2 times that of the donor O atom. The

148   crystallographic data can be found in the original CIF (as supplemental file[1]). Selected bond

149   distances are given in Table 2 and a bond-valence analysis in Table 3.

150   Attempts to refine the occupancies of the cation sites suggested full occupancies of the

151   Mn^{2+} sites (Mn1, Mn2, Mn3 and Mn4) by Mn, the Zn site by Zn and the Al site by Al. The

152   scattering powers of Mn and Fe are too similar to provide a meaningful indication of preferential

153   occupancy of Fe in any of the Mn sites; however, the high BVS for the Mn3 site of 2.12 valence

154   units (v.u.) suggests that Fe^{2+} is likely to prefer this site. The BVS for this site with occupancy

155   only by Fe^{2+} is only 1.89 v.u., suggesting that the Mn3 site is likely to be occupied roughly

156   equally by Mn and Fe. Based on the BVS values for the other Mn sites, 2.06 v.u. for Mn1, 1.99

157   v.u. for Mn2 and 2.07 v.u. for Mn4, we suggest that the 0.87 Fe apfu provided by the EPMA

158   could be allocated as follows: Mn1: $Mn_{0.80}Fe_{0.20}$ (BVS = 2.02 v.u.), Mn2: $Mn_{1.00}Fe_{0.00}$ (BVS =

159   1.99 v.u.), Mn3: $Mn_{0.55}Fe_{0.45}$ (BVS = 2.02 v.u.), and Mn4: $Mn_{0.78}Fe_{0.22}$ (BVS = 2.02 v.u.).

160   Nevertheless, the best refinement was obtained with all four Mn sites assigned full occupancies

161   by Mn only.

162

163   ATOMIC ARRANGEMENT

164   The structure of jasonsmithite (Figs. 5 and 6) contains zig–zag chains of edge–sharing

165   MnO_6 octahedra along [100]. The chains are linked into sheets parallel to {001} by sharing

166   corners with octahedra in adjacent chains and by sharing corners with peripheral PO_4 tetrahedra.

167   A ZnO_4 tetrahedron decorates the sheet, sharing three of its corners with polyhedra in the sheet;

168   its unshared fourth corner is an H_2O group. Dimers of edge–sharing AlO_6 octahedra corner link

169   to PO_4 tetrahedra in adjacent sheets, thereby linking the sheets into a framework. The framework

170   contains large channels along [100] that contain five different H_2O sites (OW25, OW26, OW27,

171   OW28, and OW29). OW25 and OW26 are fully occupied. OW27 and OW28 are only 0.710(16)

172   Å apart and OW29 is only 1.65(2) Å from an equivalent OW29 site across the 0,0,½ center of

173   symmetry. These three sites refined to close to half occupancy and were assigned half

174   occupancies in the final refinements. The OW27, OW28, and OW29 sites were the only H_2O O

175   sites for which the associated H sites could not be located.

176   While the structure of jasonsmithite is unique among natural and synthetic phases, the

177   sheet of octahedra and tetrahedra that it contains (Fig. 6) is topologically identical to those in

178   angarfite, $NaFe^{3+}_5(PO_4)_4(OH)_4(H_2O)_4$ (Kampf et al. 2012), bakhchisaraitsevite,

179    $Na_2Mg_5(PO_4)_4(H_2O)_6 \cdot H_2O$ (Liferovich et al. 2000; Yakubovich et al. 2000), liversidgeite,

180    $Zn_6(PO_4)_4(H_2O)_5 \cdot 2H_2O$ (Elliott et al. 2010), mejillonesite, $NaMg_2(PO_3OH)(PO_4)(OH)(H_5O_2)$

181 (Atencio et al. 2012), and rimkorolgite, $BaMg_5(PO_4)_4(H_2O)_7 \cdot H_2O$ (Krivovichev et al. 2002). The

182 manner in which these sheets are linked to one another differs for each of these minerals.

183

184   IMPLICATIONS

185   The structure of jasonsmithite contains 1D channels that are contained within 14-member

186 rings (14MR) comprised of six MnO_6 octahedra, four AlO_6 octahedra, and four PO_4 tetrahedra

187 (Fig. 7), which define a high-porosity framework with the potential for high molecular

188 conductivity. The 14MR are oriented parallel to the {103} plane that creates a pillared-like

189 geometry to support the Mn-sheets (cf. Clearfield and Wang 2002). The channels have side-

190 branch pockets containing extra-framework H_2O that are similar to other interrupted microporous

191 frameworks [e.g. scandium phosphates (Bull et al. 2003, Park et al. 2004)]. Calculated void space

192 (with extra-framework H_2O removed) using the CrystalMaker software yielded a void space of

193 70.2% per unit cell, and a framework density of 14.5 polyhedral atoms/1000 $Å^3$, which would

194 place it among the most porous minerals as compared to zeolites (Baerlocher et al. 2007). The

195 largest cavity is located at 0,½,0 with a diameter of 6.4 Å. The tetrahedrally coordinated P atoms

196 at sites P3 and P4 each have one oxygen (O10 and O14, respectively) that does not bridge

197 directly to another framework cation. Sites O10 and O14 form hydrogen bonds to the extra-

198 framework H_2O in the channels. Framework Zn in microporous structures has been previously

199 found to show promising catalytic activity (Orazov and Davis 2016). The presence of a hydrated

200 Zn polyhedron along the walls of the jasonsmithite channels may provide a site for catalytic

201 activity if hydrolyzed to form a Lewis acid center, and this would be worth further exploration in

202 the search of low-temperature microporous catalysts. The solvent-accessible void space is shown

203 in Figure 8.

204

210

211   REFERENCES

212   Atencio, D., Chukanov, N.V., Nestola, F., Witzke, T., Coutinho, J.M.V., Zadov, A.E., Contreira

213   Filho, R.R., and Färber, G. (2012) Mejillonesite, a new acid sodium, magnesium hydrogen

214   phosphate mineral from Mejillones, Antofagasta, Chile. American Mineralogist, **97**, 19–25.

215   Baerlocher, C., McCusker, L.B., and Olson, D.H. (2007) Atlas of Zeolite Framework Types.

216   Elsevier.

217   Bull, I., Young, V., Teat, S.J., Peng, L., Grey, C.P., and Parise, J.B. (2003) Hydrothermal

218   synthesis and structural characterization of four scandium phosphate frameworks. Chemistry

219   of Materials, **15**, 3818–3825.

220   Clearfield, A. and Wang, Z. (2002) Organically pillared microporous zirconium phosphonates.

221   Journal of the Chemical Society, Dalton Transactions, **15**, 2937–2947.

222   Elliott, P., Giester, G., Libowitzky, E., and Kolitsch, U. (2010) Description and crystal structure

223   of liversidgeite, $Zn_6(PO_4)_4 \cdot 7H_2O$, a new mineral from Broken Hill, New South Wales,

224   Australia. American Mineralogist, **95**, 397–404.

225   Ferraris G. and Ivaldi G. (1988) Bond valence vs. bond length in O…O hydrogen bonds. Acta

226   Crystallographica, **B44**, 341–344.

227   Gagné, O.C. and Hawthorne, F.C. (2015) Comprehensive derivation of bond–valence parameters

228   for ion pairs involving oxygen. Acta Crystallographica, **B71**, 562–578.

229   Higashi, T. (2001) ABSCOR. Rigaku Corporation, Tokyo.

230   Kampf, A.R., Mills, S.J., Housley, R.M., Boulliard, J.–C., and Bourgoin, V. (2012) Angarfite,

231         $NaFe^{3+}_5(PO_4)_4(OH)_4 \cdot 4H_2O$, a new mineral from the Angarf–Sud pegmatite, Morocco:

232   description and crystal structure. Canadian Mineralogist **50**, 781–791.

233   Krivovichev, S.V., Britvin, S.N., Burns, P.C., and Yakovenchuk, V.N. (2002) Crystal structure of

234   rimkorolgite, $Ba[Mg_5(H_2O)_7(PO_4)_4](H_2O)$, and its comparison with

235   bakhchisaraitsevite. European Journal of Mineralogy, **14**, 397–402.

236   Liferovich, R.P., Pakhomovsky, Ya.A., Yakubovich, O.V., Massa, W., Laajoki, K., Gehör, S.,

237   Bogdanova, A.N., and Sorokhtina, N.V. (2000) Bakhchisaraitsevite, $Na_2Mg_5[PO_4]_4 \cdot 7H_2O$, a

238   new mineral from hydrothermal assemblages related to phoscorite–carbonatite complex of the

239   Kovdor massif, Russia. Neues Jahrbuch für Mineralogie, Monatshefte, **2000**, 402–418.

240   Mandarino, J.A. (2007) The Gladstone–Dale compatibility of minerals and its use in selecting

241   mineral species for further study. Canadian Mineralogist, **45**, 1307–1324.

242   Orazov, M. and Davis, M.E. (2016) Catalysis by framework zinc in silica-based molecular

243   sieves. Chemical Science, **7**, 2264–2274.

244   Park, H., Bull, I., Peng, L., Young, V. G., Grey, C. P., and Parise, J. B. (2004) Synthesis and

245   structure determination of a new organically templated scandium fluorophosphate framework

246   and its indium analogue. Chemistry of Materials, **16**, 5350–5356

247   Pouchou, J.–L. and Pichoir, F. (1991) Quantitative analysis of homogeneous or stratified

248   microvolumes applying the model "PAP." In: Heinrich, K.F.J. and Newbury, D.E. (eds)

249   Electron Probe Quantitation. Plenum Press, New York, pp. 3l–75.

250   Rakovan, J., Barnett, B., and White, J.S. (2016) Fluorapatite from the Foote mine, Kings

251   Mountain, North Carolina. Rocks & Minerals, **91**, 251–256.

252   Sheldrick, G.M. (2015a) SHELXT – Integrated space–group and crystal–structure determination.

253   Acta Crystallographica, **A71**, 3–8.

254   Sheldrick, G.M. (2015b) Crystal Structure refinement with SHELX. Acta Crystallographica,

255   **C71**, 3–8.

256   Yakubovich, O.V., Massa, W., Liferovich, R.P., and Pakhomovsky, Y.A. (2000) The crystal

257   structure of bakhchisaraitsevite, $[Na_2(H_2O)_2]\{(Mg_{4.5}Fe_{0.5})(PO_4)_4(H_2O)_5\}$, a new mineral

258   species of hydrothermal origin from the Kovdor phoscorite–carbonatite Complex, Russia.

259   Canadian Mineralogist, **38**, 831–838.

260

261   **Endnote:**

262   [1]Deposit item AM-20-XXXXX, Supplemental tables and CIF. Deposit items are free to all

263   readers and found on the MSA website, via the specific issue's Table of Contents (go to

264   http://www.minsocam.org/MSA/AmMin/TOC/2020/Xxx2020_data/ Xxx2020_data.html).

265   FIGURE CAPTIONS

266   Figure 1. Crystal drawing of jasonsmithite; clinographic projection in non–standard orientation, **a**

267   vertical.

268   Figure 2. Jasonsmithite on holotype specimen (LACMNH 74374); FOV 0.84 mm across.

269   Figure 3. Background–corrected Raman spectrum of jasonsmithite recorded using a 532 nm laser.

270   The recorded spectrum is in dark blue; the fitted bands are in various colors; the sum of

271   the fitted bands is in red.

272   Figure 4. The observed powder diffraction pattern compared with the pattern simulated from the

273   lines calculated from the crystal structure.

274   Figure 5. Crystal structure of jasonsmithite viewed down **a**. The O atoms of the channel H_2O

275   groups (OW25, OW26, OW27, OW28, and OW29) are numbered.

276   Figure 6. The sheet of octahedra and tetrahedra in the jasonsmithite structure viewed down **c***

277   with **a** vertical and **b** horizontal. Except for minor geometric deviations, this sheet is

278   identical to those in angarfite, bakhchisaraitsevite, and mejillonesite.

279   Figure 7. The 14-member ring (14MR) in the structure of jasonsmithite viewed along **a**.

280   Figure 8. Map of calculated solvent-accessible void space to a distance of 1.2 Å from the nearest

281   van der Waals surface. Blue shows inner surface of channel. Grey spheres show areas of

282   largest cage volume. The unit cell outline is shown.

283
284

285   Table 1. Analytical data (wt.%) for jasonsmithite.

286

Constituent	Mean	Range	SD	Standard
MnO	25.09	23.99 – 26.69	0.83	rhodonite
FeO	7.17	5.89 – 8.03	0.80	hematite
ZnO	9.75	8.69 – 10.72	0.68	syn. ZnO
Al_2O_3	5.69	5.59 – 5.80	0.06	sanidine
P_2O_5	32.48	31.58 – 33.18	0.54	apatite
H_2O*	22.72			
Total	102.90			

287   * Based on the structure

288

289

290

291

292   Table 2. Selected bond distances (Å) for jasonsmithite.
293

Mn1–O12	2.117(4)	Mn4–O2	2.084(4)	P1–O1	1.515(4)
Mn1–O1	2.130(3)	Mn4–O7	2.122(3)	P1–O2	1.519(4)
Mn1–O15	2.131(4)	Mn4–O16	2.161(3)	P1–O3	1.551(3)
Mn1–O7	2.170(3)	Mn4–O11	2.177(3)	P1–O4	1.571(4)
Mn1–OW21	2.214(4)	Mn4–OW24	2.270(4)	<P1–O>	1.539
Mn1–OW22	2.423(4)	Mn4–OW22	2.350(4)		
<Mn1–O>	2.198	<Mn4–O>	2.194	P2–O5	1.510(4)
				P2–O6	1.528(4)
Mn2–O3	2.114(3)	Zn–O13	1.922(4)	P2–O7	1.533(3)
Mn2–O6	2.125(4)	Zn–O4	1.978(3)	P2–O8	1.554(3)
Mn2–O11	2.139(3)	Zn–OW18	1.990(4)	<P2–O>	1.531
Mn2–O16	2.175(3)	Zn–O8	1.990(4)		
Mn2–OW21	2.279(4)	<Zn–O>	1.970	P3–O9	1.517(4)
Mn2–OW23	2.470(4)			P3–O10	1.535(4)
<Mn2–O>	2.217	Al–O9	1.829(4)	P3–O11	1.542(3)
		Al–O5	1.845(4)	P3–O12	1.543(4)
Mn3–O12	2.117(4)	Al–OH17	1.899(4)	<P3–O>	1.534
Mn3–O3	2.160(3)	Al–OW20	1.936(4)		
Mn3–O8	2.165(3)	Al–OW19	1.940(4)	P4–O13	1.542(4)
Mn3–O15	2.189(4)	Al–OH17	1.941(4)	P4–O14	1.542(4)
Mn3–OW23	2.193(4)	<Al–O>	1.898	P4–O15	1.543(4)
Mn3–OW24	2.228(4)			P4–O16	1.543(3)
<Mn3–O>	2.175			<P4–O>	1.543

317

318   *Hydrogen bonds*

D–H···A	D–H	H···A	D···A	<DHA
OH17–H17···O1	0.81(3)	1.99(3)	2.799(5)	171(6)
OW18–H18A···OH17	0.85(3)	1.89(3)	2.731(5)	172(6)
OW18–H18B···OW25	0.81(3)	2.24(4)	2.911(8)	141(6)
OW19–H19A···O4	0.82(3)	1.92(3)	2.730(5)	167(5)
OW19–H19B···O4	0.81(3)	1.84(3)	2.644(5)	172(6)
OW20–H20A···O6	0.84(3)	1.85(3)	2.685(5)	170(6)
OW20–H20B···OW26	0.78(3)	1.96(3)	2.735(7)	176(7)
OW21–H21A···O14	0.84(3)	1.90(3)	2.706(5)	161(5)
OW21–H21B···O10	0.82(3)	1.85(3)	2.641(5)	164(5)
OW22–H22A···OW27	0.83(3)	1.98(3)	2.801(16)	170(6)
OW22–H22A···OW28	0.83(3)	1.91(4)	2.715(15)	163(5)
OW22–H22B···O6	0.82(3)	2.23(3)	3.043(5)	168(6)
OW23–H23A···O2	0.82(3)	1.89(3)	2.703(5)	171(6)
OW23–H23B···OW25	0.82(3)	1.89(3)	2.695(7)	166(6)
OW24–H24A···O10	0.83(3)	1.95(3)	2.709(5)	153(5)
OW24–H24B···O14	0.81(3)	1.85(3)	2.602(5)	154(6)
OW25–H25B···OW26	0.84(3)	2.52(4)	3.304(11)	156(8)

337	OW25–H25B⋯OW29	0.84(3)	2.33(7)	2.908(15)	126(7)
338	OW26–H26A⋯O10	0.83(3)	1.86(3)	2.677(7)	167(10)
339	OW26–H26B⋯OW27	0.84(3)	2.36(8)	2.976(16)	131(8)
340	OW26–H26B⋯OW29	0.84(3)	2.25(6)	3.005(15)	150(10)

341

342   Table 3. Bond–valence analysis for jasonsmithite. Values are expressed in valence units.
343

	Mn1	Mn2	Mn3	Mn4	Al	Zn	P1	P2	P3	P4	Hydrogen bonds	sum
O1	0.39						1.31				0.18	1.89
O2				0.44			1.30					1.74
O3		0.41	0.37				1.20					1.97
O4						0.46	1.14				0.21, 0.26	2.08
O5					0.58			1.33				1.91
O6		0.40						1.27			0.23, 0.12	2.02
O7	0.36			0.40				1.26				2.01
O8			0.36			0.45		1.19				2.00
O9					0.61				1.31			1.91
O10									1.25		0.24, 0.26, 0.22	1.97
O11		0.38		0.35					1.23			1.96
O12	0.40		0.40						1.23			2.03
O13						0.54				1.23		1.77
O14										1.23	0.22, 0.29	1.74
O15	0.39		0.34							1.23		1.96
O16		0.35		0.36						1.23		1.94
OH17					0.51 0.46						−0.18, 0.21	1.00
OW18						0.45					−0.21, −0.15	0.09
OW19					0.46						−0.21, −0.26	−0.01
OW20					0.46						−0.23, −0.21	0.01
OW21	0.32	0.27									−0.22, −0.26	0.11
OW22	0.19			0.23							−0.22, −0.12	0.08
OW23		0.17	0.34								−0.23, −0.23	0.06
OW24			0.31	0.28							−0.22, −0.29	0.08
OW25											−0.09, −0.15, 0.15	−0.09
OW26											−0.24, 0.21, 0.09	0.06
sum	2.06	1.99	2.12	2.07	3.07	1.90	4.96	5.05	5.01	4.91		

344   Bond–valence parameters are from Gagné and Hawthorne (2015). Hydrogen–bond strengths
345   based on O–O bond lengths from Ferraris and Ivaldi (1988). Half–occupied OW27, OW28, and
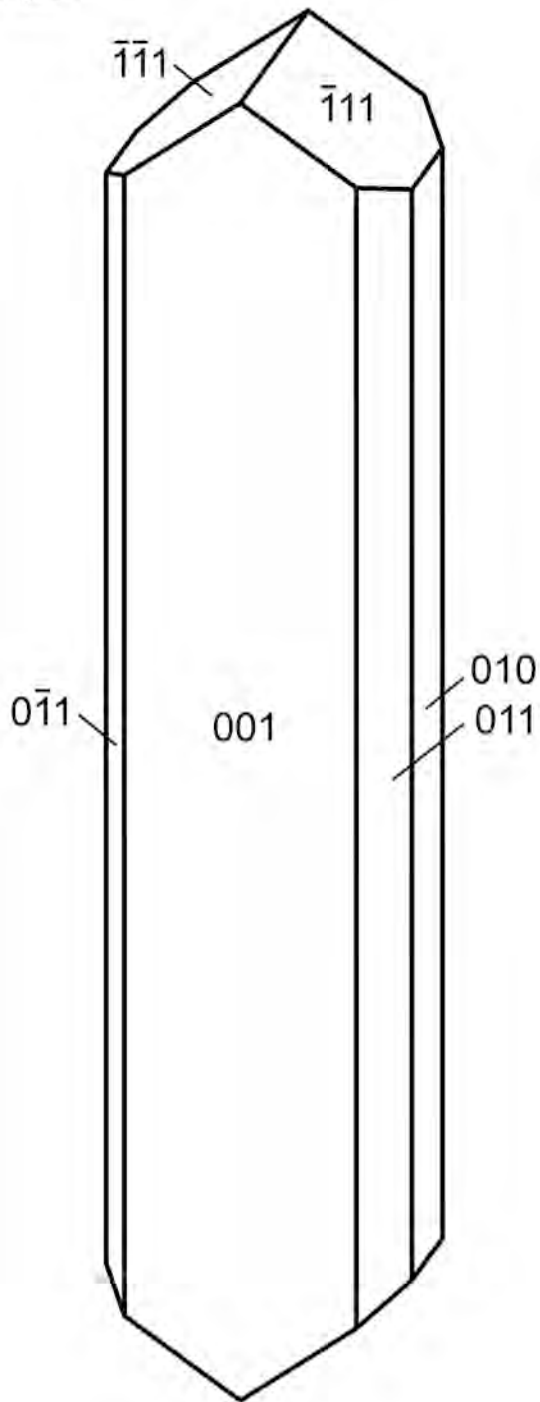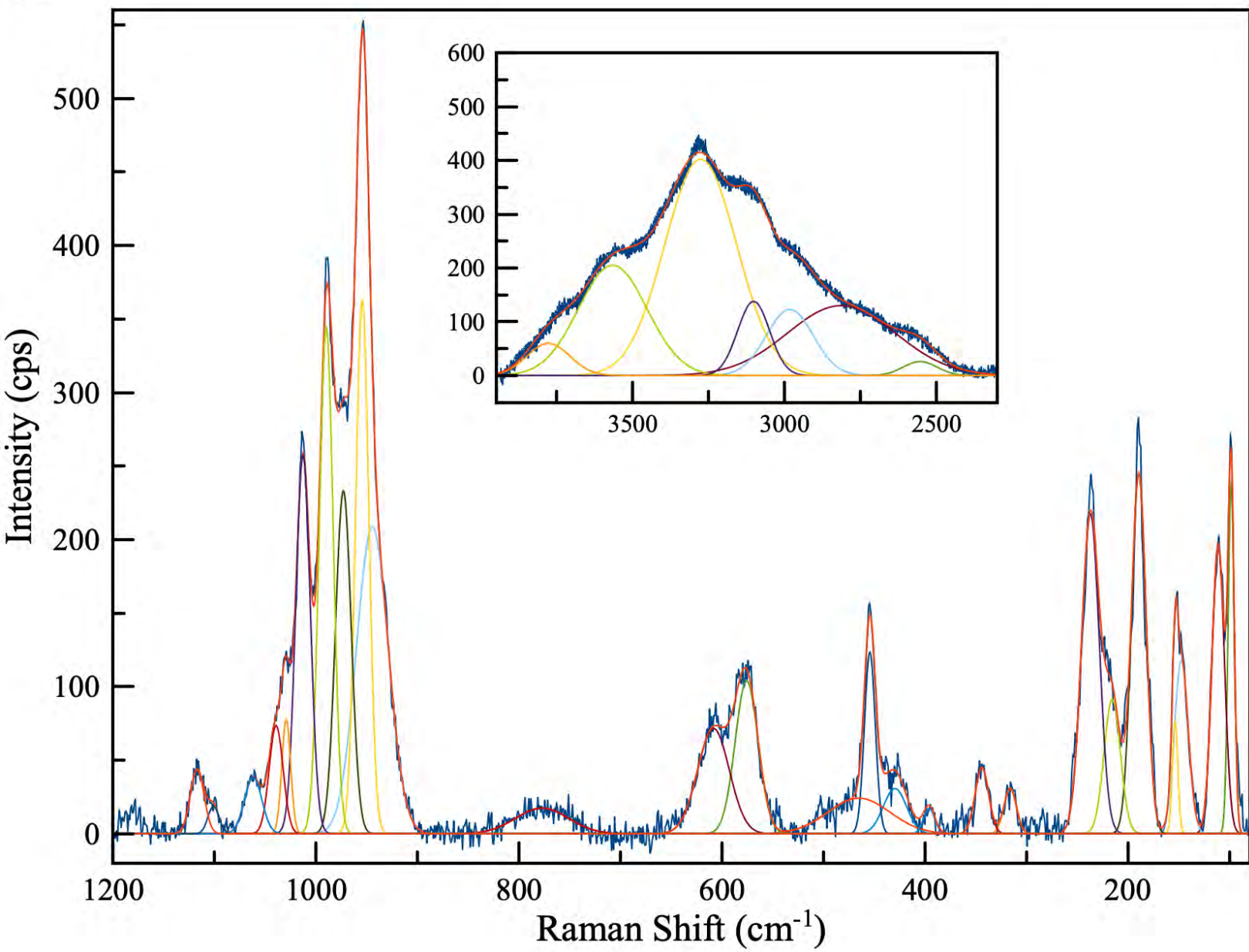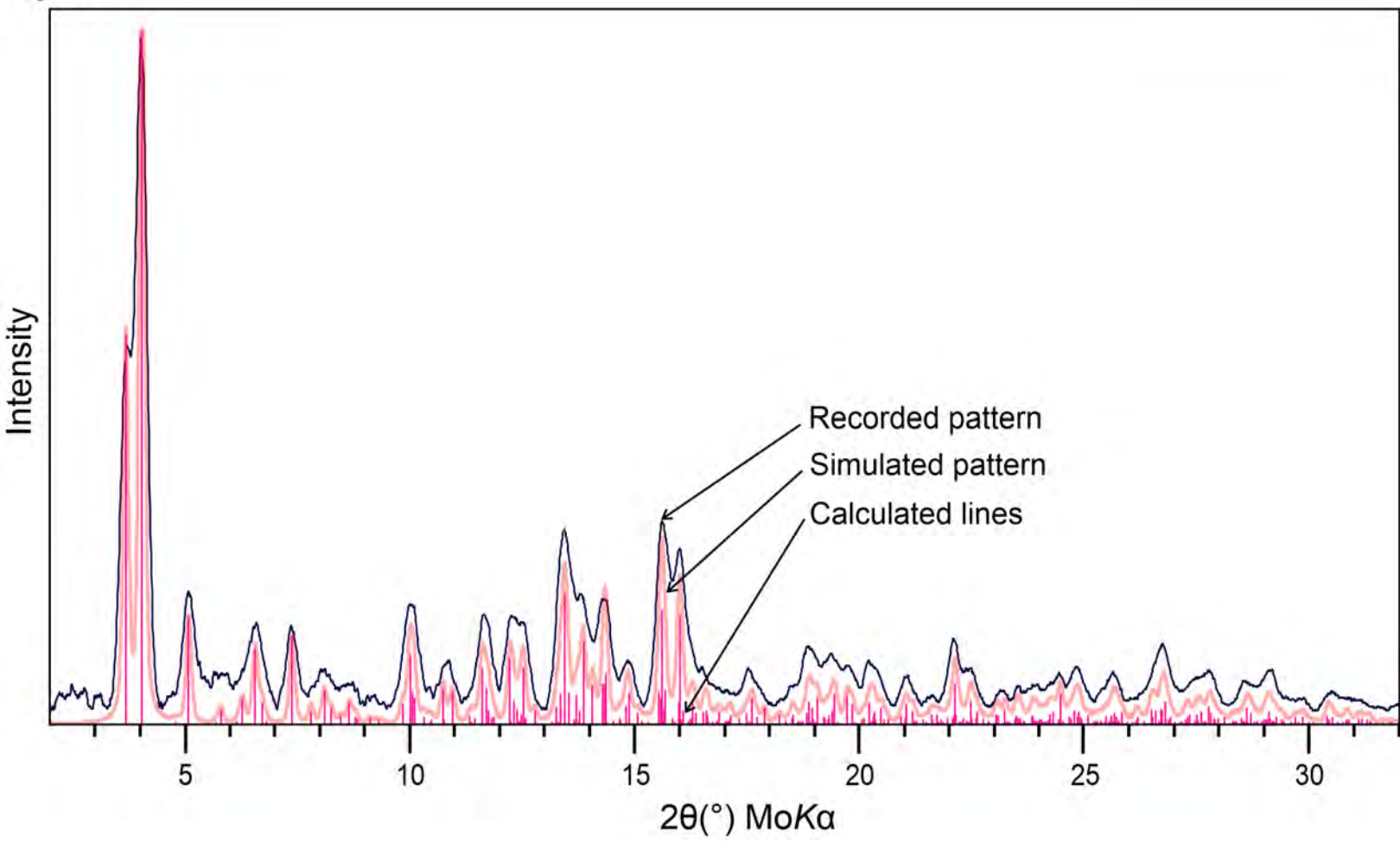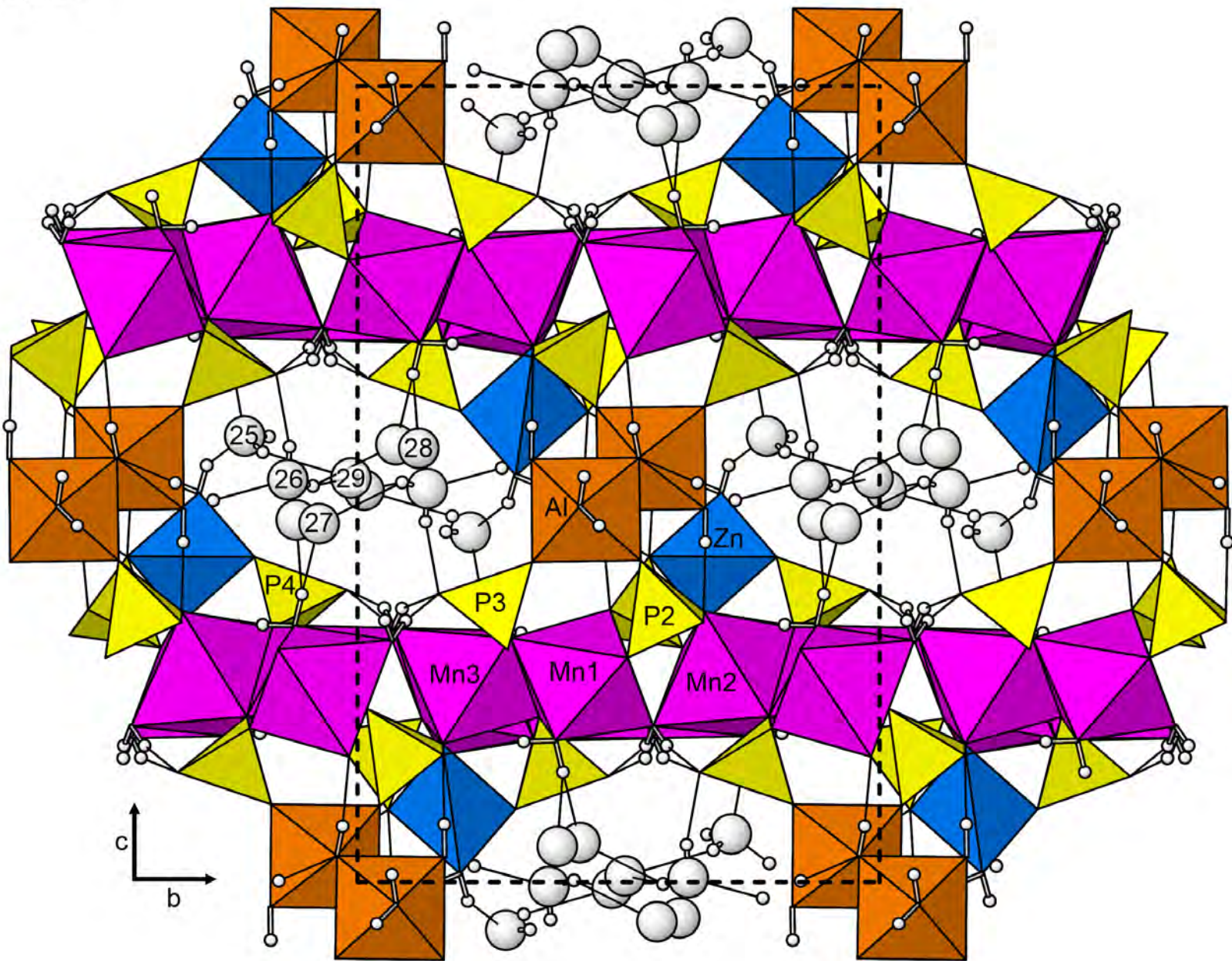346   OW29 sites are not included.
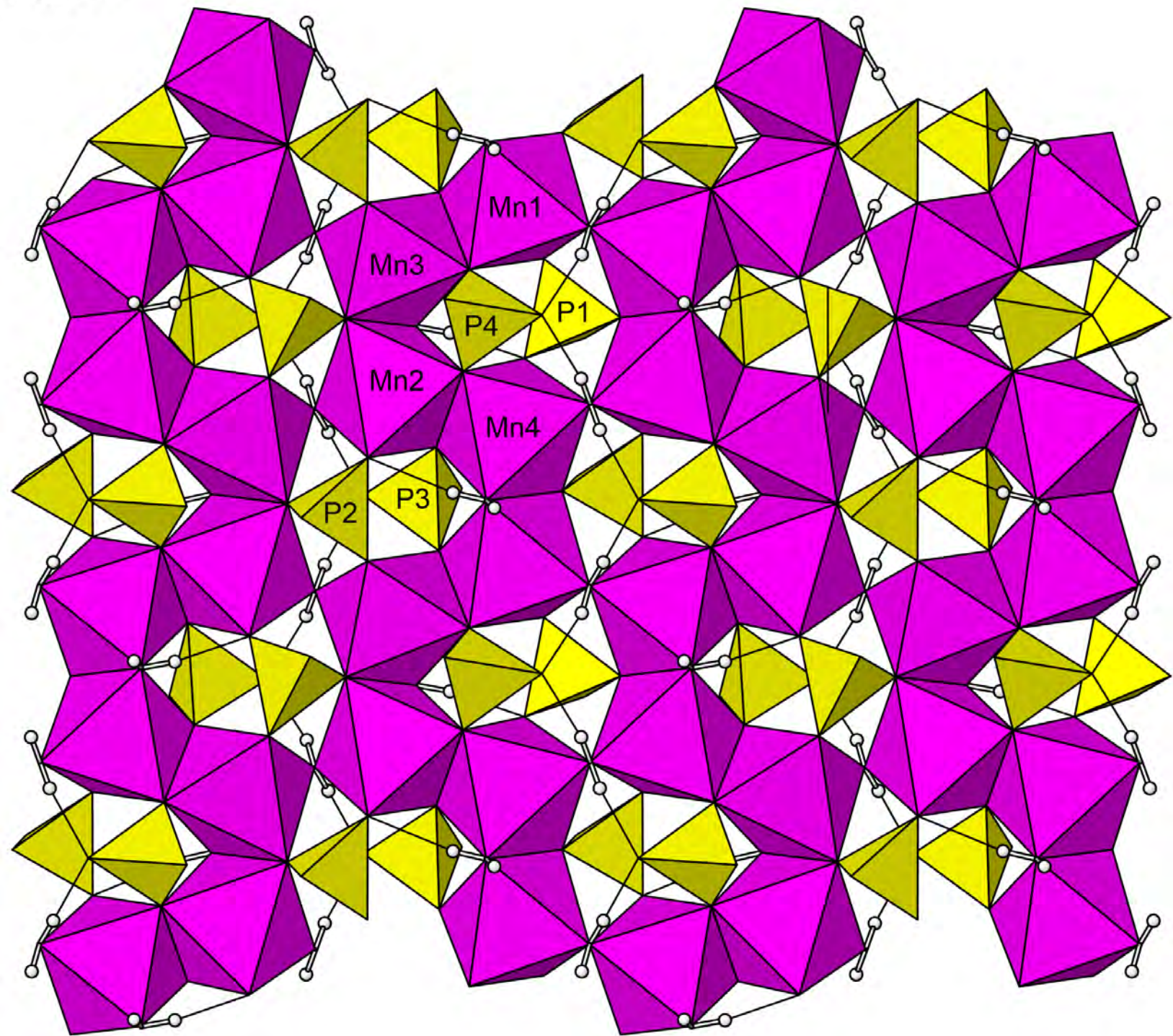347
348

Figure 1

Figure 2

Figure 3

Figure 4

Figure 5

Figure 6

Figure 7

Figure 8